Thermomagnetic convection control strategies for electromagnetic devices immersed in a ferrofluid

Sleimane Nasser El Dine, Xavier Mininger, Caroline Nore

Journal Pre-proof

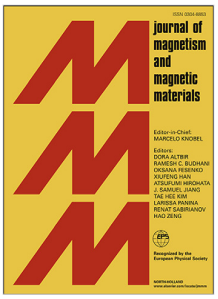

Thermomagnetic convection control strategies for electromagnetic devices immersed in a ferrofluid

Sleimane Nasser El Dine, Xavier Mininger, Caroline Nore

PII: S0304-8853(24)00167-7
DOI: https://doi.org/10.1016/j.jmmm.2024.171876
Reference: MAGMA 171876

To appear in: *Journal of Magnetism and Magnetic Materials*

Received date : 23 May 2023
Revised date : 17 January 2024
Accepted date : 15 February 2024

Please cite this article as: S. Nasser El Dine, X. Mininger and C. Nore, Thermomagnetic convection control strategies for electromagnetic devices immersed in a ferrofluid, *Journal of Magnetism and Magnetic Materials* (2024), doi: https://doi.org/10.1016/j.jmmm.2024.171876.

Thermomagnetic Convection Control Strategies for Electromagnetic Devices Immersed in a Ferrofluid

Sleimane Nasser El Dine[1], Xavier Mininger[1], and Caroline Nore[2]
[1]Université Paris-Saclay, CentraleSupélec, Sorbonne Université, CNRS, Laboratoire de Génie Electrique et Electronique de Paris, 91192 Gif-sur-Yvette, France
sleimane.nassereldine@geeps.centralesupelec.fr, xavier.mininger@geeps.centralesupelec.fr
[2]Université Paris-Saclay, CNRS, LISN, 91405 Orsay, France
caroline.nore@lisn.upsaclay.fr

This paper presents new control strategies for improving the thermomagnetic convection intensity in electromagnetic devices. The system consists of a winding prototype immersed in a ferrofluid solution based on magnetic nanoparticles. The whole system is exposed to an external magnetic field generated by an annular magnet placed against the tank. When possible, experimental results are compared with numerical ones obtained using the finite element method in a 2D-axisymmetric setting. The first control strategy consists of assessing the impact of Curie's temperature on heat removal. Numerical calculations show that the maximum winding temperature decreases by $2.2\,^{\circ}\mathrm{C}$ with the use of magnetic nanoparticles with the lowest Curie temperature. Employing an auxiliary magnetic field may be another method for monitoring the thermomagnetic convection. The number of streamlines increases in the upper part of the tank due to the intensification of the magnetic force at the top of the winding. It is shown that magnetization, orientation, and location of the magnet play a crucial role in maximizing heat transfer inside the tank. The experiment shows a temperature decrease of 9°C at the top of the winding if an external magnetic field is applied.

***Index Terms*—Thermomagnetic Convection, Electromagnetic device, Magnet, Curie Temperature, Finite Elements Method, Ferrofluid.**

I. Introduction

THE aim of this paper is to evaluate different original approaches in the context of improving thermomagnetic convection in electrical transformers. Thermomagnetic convection is a phenomenon which arises in a ferrofluid where both a temperature gradient and a magnetic field intensity gradient are applied [1], [2], [3], [4], [5], [6], [7], [8], [9]. The crucial point is that the variations of the magnetic body force applied to the fluid, being a function of the temperature and the magnetic field strength, can develop and lead to a convective flow. This phenomenon was investigated in prototype transformers [10], [11], [12], [13], [14], [15].

A recent study presents a fully thermal-fluid-magnetic coupling method based on the 3D finite elements to study the cooling efficiency inside a ferrofluid-based transformer [16]. This paper shows the benefit of thermomagnetic convection on transformer cooling. A 400/230V transformer with a non-axisymmetric ferromagnetic core has been modeled. The maximum temperature in the primary winding is reduced by $10\,^{\circ}\mathrm{C}$ due to the ferrofluid flow channeling the gap between conductors.

Plenty of papers have reported on thermomagnetic convection and its impact on the cooling of electromagnetic devices. Some authors proposed using external sources of magnetic fields, for instance, permanent magnets, to maximize the heat transfer through the cooling liquid by modifying the distribution of leakage magnetic flux [17], [18]. These studies showed improved thermomagnetic convection numerically when auxiliary magnets are used. However, no experimental validations have been performed at this level to confirm the benefit of modifying magnetic field distributions in ferrofluid liquids and their influence on the heat transfer process. Other studies assessed the heat transfer through electromagnetic devices when oscillating magnetic fields are applied in the cooling solution [19], [20], [21]. Studies have shown that thermomagnetic convection is thus improved due to the periodic vortex that appeared in the ferrofluid and enhanced the cooling process. These results remain questionable since the application of such an oscillating magnetic field could affect the dielectric properties of ferrofluids which are mandatory for electric transmission reasons. In addition, ferrofluid with different Curie temperatures of magnetic nanoparticles and under an oscillating magnetic field shall be investigated to confirm its benefit on cooling such devices.

In this paper, an assessment of the heat transfer for the current electric prototype has been performed with different Curie temperatures of dielectric liquid. Furthermore, a deep investigation of the cooling process for a ferrofluid-immersed solenoid is reported while using external magnets. Changes in the magnetization direction of the magnet, positioning, and orientation are also considered.

Memory resources and computation time associated with numerical simulations of the multiphysics coupling directly on actual transformer geometries are not compatible with a heat exchange optimization process. As a consequence, all the studies are first tested in this paper with the consideration of a simplified electromagnetic setup: a ferrofluid-immersed solenoid. We have already shown in [22] that using ferrofluid in a solenoid setup presents a benefit in terms of cooling.

Indeed, the maximum temperature of the solenoid is lowered thanks to thermomagnetic convection. This paper explores additional considerations for optimizing the cooling process without adding another energy source. As a first step, the Curie temperature of the magnetic nanoparticles in the ferrofluid suspension is varied to determine numerically its impact on the thermomagnetic convection. In [22], we also introduced the theoretical impact of a magnet that modifies the magnetic field distribution. In this paper, different configurations of an auxiliary magnet -location, magnetization orientation, and amplitude of the remanent magnetization- are considered to evaluate both numerically and experimentally the effect of the magnet on heat transfer.

II. Experimental Setup, Governing Equations and Numerical Modeling

In this section, the principle of thermomagnetic convection, the experimental setup, the governing equations and the approximation technique proposed to consider this multiphysics problem are briefly described. Only the essential points of the associated numerical modeling approach are exposed, as more details can be found in our previous paper [22].

A. Thermomagnetic Convection

The ferrofluid magnetization is given by Langevin's theory for linear magnetic material [23]:

$$\mathbf{M} = \chi(T)\mathbf{H}, \tag{1}$$

where $\mathbf{M}$ is the ferrofluid magnetization, T the temperature in K, and $\mathbf{H}$ the magnetic field. χ is the ferrofluid magnetic susceptibility given by Finlayson [1] and defined by:

$$\chi(T) = \frac{\phi\mu_0\pi d^3 M_{s,p}^2(T)}{18k_BT}, \quad \frac{M_{s,p}(T)}{M_0} = 1 - \left(\frac{T}{T_c}\right)^{\frac{3}{2}}, \tag{2}$$

where ϕ is the volume fraction of magnetic nanoparticles, μ_0 the free space magnetic permeability, d the mean diameter of nanoparticles, $M_{s,p}(T)$ the saturation magnetization of the particle dependent on temperature, k_B the Boltzmann constant, M_0 the saturation magnetization of the particles at 0 K, and T_c the Curie temperature of the magnetic material. The most popular model for the magnetic body force is the Kelvin force given in [24]. Using the collinearity between **M** and **H** and Langevin's formula, it can be written as:

$$\mathbf{F}_m = \mu_0\chi(T)\boldsymbol{\nabla}\frac{H^2}{2} \tag{3}$$

where $H = \|\mathbf{H}\|$. This expression can help understanding the thermomagnetic convection: the magnetization intensity being mainly inversely proportional to the temperature (see eq.(2)), a cold ferrofluid is more strongly magnetized [25] and the magnetic Kelvin force is greater in a cold region than in a hot one [26]. If the magnetic field source is near the heat source, a convective flow appears: the cold more attracted fluid moves toward the heat source and forces away the hot less attracted fluid.

B. Experimental Bench

The experimental setup is based on a copper solenoid immersed in a cobalt ferrite ($CoFe_2O_4$) ferrofluid ($\phi = 5.4\%$) contained in an aluminum tank, which is closed at the top by a PVC (PolyVinyl Chloride) plug as shown in Fig. 1. Two thermocouples are used to measure the temperature at the top surface of the solenoid and in the fluid. An annular magnet with a rectangular cross-section and an axial magnetization can be positioned against the tank, to study the impact of the external field provided by the magnet. The dimensions of the experimental setup are given in Table 1.

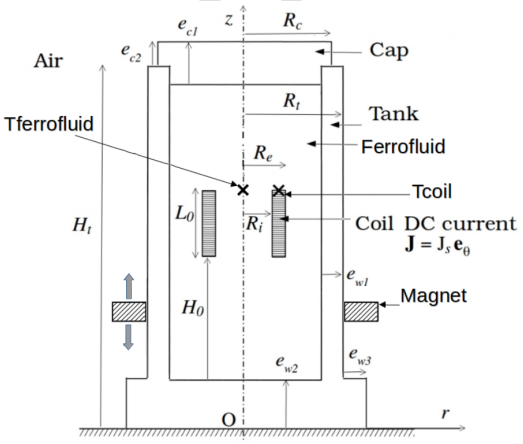

(a)

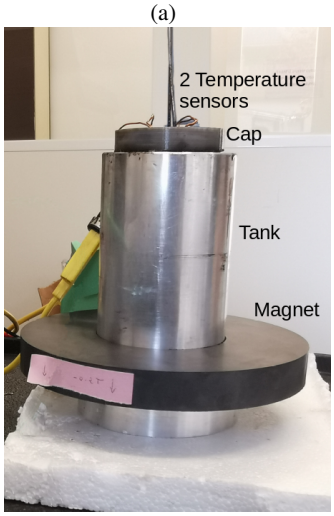

(b)

Fig. 1: Sketch of the setup geometry (a) and experimental tank with its surrounding magnet (b).

C. Governing Equations and material properties

The ferrofluid is treated as a continuous homogeneous fluid with an incompressible Newtonian fluid behavior. Its motion is described by the incompressible Navier–Stokes equations:

$$\begin{cases} \boldsymbol{\nabla}\cdot\mathbf{u} = 0, \\ \rho\partial_t\mathbf{u} + \rho(\mathbf{u}\cdot\boldsymbol{\nabla})\mathbf{u} + \boldsymbol{\nabla}p - \eta(T_{ext})\boldsymbol{\nabla}^2\mathbf{u} = \\ \quad -\rho\mathbf{g}\beta(T - T_{ext}) + \mathbf{F}_m, \end{cases} \tag{4}$$

Parameter	H_t	R_t	e_{w1}	e_{w2}	e_{w3}	H_0
Value (cm)	12.5	3.1	1	2	1	3.9
Parameter	L_0	R_i	R_e	R_c	e_{c1}	e_{c2}
Value (cm)	2.1	0.8	1.175	2.6	2	1

TABLE 1: Experimental setup dimensions

with $\mathbf{u}$ the velocity vector, T_{ext} the reference temperature, $\eta(T_{ext})$ the dynamic viscosity of the ferrofluid defined in [23], p the pressure, T the temperature, ρ the reference density at $T = T_{ext}$, β the thermal expansion coefficient and $\mathbf{g}$ the gravity vector. The two terms on the right-hand side of the momentum equation are respectively the buoyancy force considering the Boussinesq approximation and the Kelvin magnetic body force (in N/m^3) defined in Eq. (3). The parameters for the magnetic susceptibility to compute the Kelvin force are $\phi = 5.4\%$, $d = 16\,\text{nm}$, $M_0 = 3.87 \times 10^5\,\text{Am}^{-1}$. The Curie temperature T_c will be given different values in the following sections.

The heat equation describes the heat transfer process that occurs in the ferrofluid:

$$\rho c \partial_t T + \rho c(\mathbf{u} \cdot \boldsymbol{\nabla})T = \boldsymbol{\nabla} \cdot (\lambda \boldsymbol{\nabla} T) + Q, \tag{5}$$

where c is the specific heat capacity at constant pressure, λ the thermal conductivity and Q the volumic heat source dissipated by Joule effect in the coil ($Q = 6.14 \times 10^5\,\text{W/m}^3$) and given by $\frac{1}{\sigma} J_s^2$ where σ is the copper electrical conductivity ($\sigma = 5.998 \times 10^7\,\text{Sm}^{-1}$), and J_s the current density in the coil ($J_s = 3.35 \times 10^6\,\text{Am}^{-2}$). The corresponding electrical current in the coil is $I = 4$ A, the number of turns is $N = 33$, and the total coil resistance at the reference temperature is $R_t = 94\,\text{m}\Omega$. Joule losses are calculated to be $P_J = 3\,\text{W}$. The material properties of the solenoid are obtained by classical homogenization laws considering the copper and the ferrofluid [26]. The ambient air is characterized by the exterior temperature $T_{\text{ext}} = 288.15\,\text{K}$. Thermophysical properties used in the numerical simulations are reported in Table (2).

The computed electromagnetic field is assumed to be steady, and the ferrofluid magnetization is considered instantaneously aligned with the magnetic field [27, p. 22-23]. The magnetostatic equations are given by:

$$\begin{cases} \boldsymbol{\nabla} \times \mathbf{H} = \mathbf{J}, \\ \boldsymbol{\nabla} \cdot (\mu \mathbf{H}) = 0, \end{cases} \tag{6}$$

with $\mathbf{J} = J_s \mathbf{e}_\theta$ and μ the magnetic permeability of the ferrofluid $\mu = \mu_0(1 + \chi(T_{ext}))$ as the change in the permeability of the ferrofluid with increasing temperature affects the magnetic field distribution only slightly.

D. Numerical Modeling

The governing equations and material properties are inserted in a multiphysics numerical model: the magnetic problem is simulated first, and a transient thermofluidic study is next performed considering a strong coupling between thermal and fluid flow physics. This model gives complementary information to those obtained by the experiment, as we can analyze precisely the local distributions of the physical quantities involved. The maximum temperature of the windings, which is a fundamental quantity for the design of electromagnetic devices, can also be obtained. Thus, the commercial software COMSOL multiphysics is used to perform 2D axisymmetric simulations using cylindrical coordinates (r, z). The model of the overall setup is shown in Fig. 2. Comparing to our previous study [22], an air volume is added around the test cell to ensure the closure of the magnetic field lines for the magnetic computation with the presence of the magnet.

Properties	Cu	Al	PVC	Solenoid	Ferrofluid
Density (kg/m^3)	8933	2700	1400	3964	1045
Therm. expansion (/K)	-	-	-	-	0.0007
Heat capacity (J/K·kg)	385	945	1000	616	1775
Therm. Cond. (W/m·K)	401	201	0.16	0.388	0.1785
Dyn. viscosity (Pa.s)	-	-	-	-	0.0703

TABLE 2: Thermophysical properties

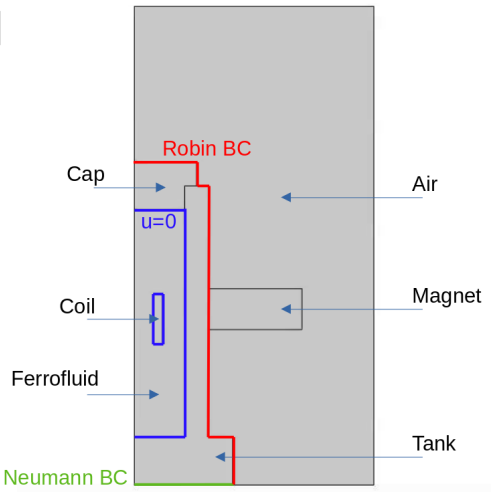

Fig. 2: 2D axisymmetric numerical model in (r, z) coordinates.

The constitutive law for the magnet is given by:

$$\mathbf{B} = \mu_0 \mathbf{H} + \boldsymbol{B_r}, \tag{7}$$

where $\boldsymbol{B_r}$ is the remanent flux density.

The magnetic vector potential $\mathbf{A}$ is used to solve the magnetostatic problem with magnetic field $\mathbf{H} = (\boldsymbol{\nabla} \times \mathbf{A})/\mu$. The associated boundary condition $\mathbf{A} \times \mathbf{n} = \mathbf{0}$ is enforced on the air boundaries. The non-slip boundary condition $\mathbf{u} = \mathbf{0}$ is applied at the border of the fluid domain (see blue lines on Fig. 2). The air convection at the top and on the lateral wall of the PVC-Aluminium tank is modeled by using a Robin boundary condition for the temperature:

$$-\lambda \nabla T \cdot \mathbf{n} = h(T - T_{ext}), \tag{8}$$

where h ($= 6.5$ W.m^{-2}K^{-1}) is the convection coefficient, and $\mathbf{n}$ is the outer unit normal vector, see red lines in Fig. 2. The system is placed in the ambient air, so natural convection is established between the tank and the environment, thanks to the temperature difference between both. As a result, the heat exchange coefficient h will be between 5 and 25 (W.m^{-2}K^{-1}). In this experiment, h is an optimized value that depends on experimental tests carried out at ambient temperature $T = 295$ K. The homogeneous Neumann boundary condition $\partial_z T = 0$ is enforced at the bottom of the tank, represented by the green line on the figure. The initial conditions are $\mathbf{u} = \mathbf{0}$ and $T = T_{ext}$. The total meridian mesh contains 47679 elements and 150 kDoFs, and is refined around the solenoid to accurately simulate the fluid flow. The four corners of the coil are slightly smoothed to best represent the actual winding.

III. Results

This section describes different attempts to improve heat transfer in the simplified solenoid configuration. The validation of the numerical approach that has been developed can be found in [22] for the initial configuration with only the coil, i.e. without the presence of the magnet.

A. *Influence of the Curie Temperature on Heat Transfer*

From experimental tests, previous studies [28], [11], [12] have recommended that the Curie temperature of ferromagnetic particles seeding the ferrofluid should be comparable to the device's operating temperature. With low Curie temperature, stronger spatial variations of the ferrofluid magnetization are indeed expected, leading to an amplified convection effect. One way to understand such an effect is to analyze the magnetic force expression in eq.(3): when magnetization variations are increased, variations of $\chi(T)$ are higher, and the gradient of the magnetic force is stronger. To better understand the origin and accurately quantify the benefits of ferromagnetic nanoparticles with low Curie temperature for the present application, the time evolution of the temperature at the top of the solenoid is simulated using ferrofluids with various Curie temperatures. Velocity and temperature distributions are also compared to analyse how this parameter impacts the fluid flow. For this part, the original numerical model validated in [22] can directly be used, with only a modification of T_c in the expression of the particle saturation magnetization used for the computation of the Kelvin force. As previously detailed (see eq.(2)), the saturation magnetization of the magnetic nanoparticles is given by the Bloch's law [29]:

$$M_{s,p}(T) = \begin{cases} M_0 \left(1 - \left(\dfrac{T}{T_c}\right)^{\frac{3}{2}}\right) & \text{if } T \leq T_c, \\ 0 & \text{if } T \geq T_c \end{cases} \tag{9}$$

For this study, four cases are considered for the Curie temperature: $T_c = 793$ K, $T_c = 593$ K, $T_c = 393$ K and an "infinite" Curie temperature, equivalent to a constant $M_{s,p}$. For each case, the value of M_0 is adapted in order to obtain the same value for $M_{s,p}$ at room temperature, i.e. 20 °C as presented on Fig. 3(a). The numerical results show that the temperature at the top of the solenoid (1 cm, 8 cm) at steady state (for $t > 20\,000$ s) is lower when the Curie temperature decreases, see Fig. 3(b). The maximum decrease is then of 2.8 °C for $T_c = 393$ K.

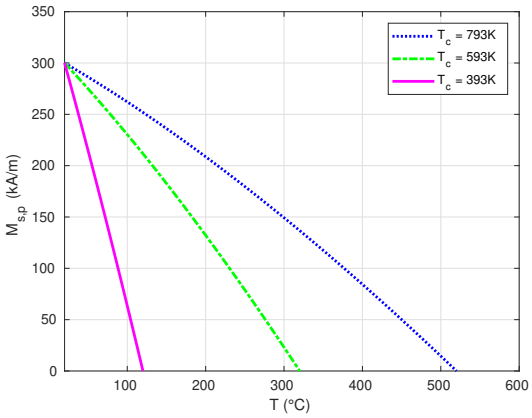

(a) Bloch's law for saturation magnetization at various Curie temperatures.

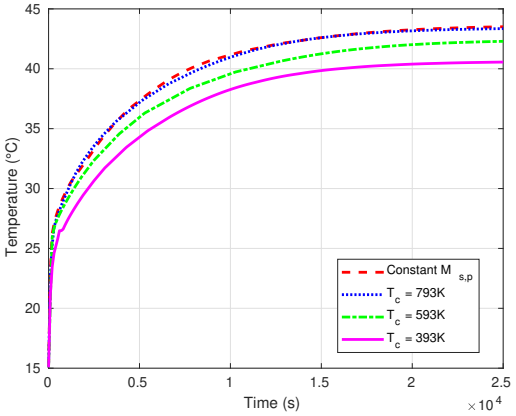

(b) Temperature on the top of the solenoid versus time using ferrofluids with various Curie temperatures.

Fig. 3: Curie temperature impacts.

To analyse the reasons for this decrease, a comparison of the velocity and temperature distributions is proposed between the case with the initial ferrofluid (Fig. 4) and the ferrofluid with $T_c = 393$ K (Fig. 5). From these results, one can deduce that the temperature decrease is related to the maximum velocity that is 2.2 times greater in the second case. However, regarding the maximum temperature of the windings, the decrease is slightly smaller than the one obtained at the coil sensor with only 1.1 °C. In any case, the conclusion here is that magnetic particles with low Curie temperature should indeed be considered for ferrofluid application in transformer cooling because they increase thermomagnetic convection.

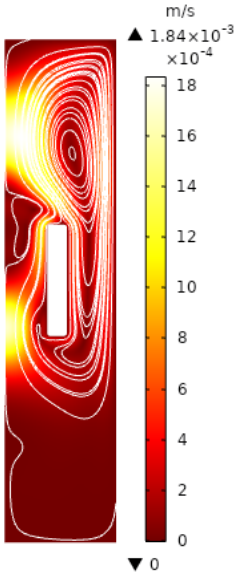

(a) Velocity streamlines.

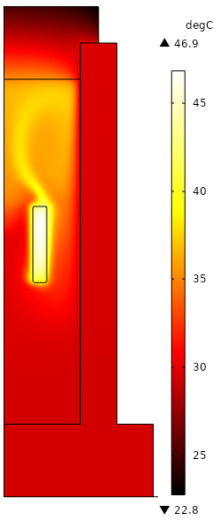

(b) Temperature.

Fig. 4: Distribution of the velocity streamlines (a) and temperature field (b) at $t = 25\,000\,\mathrm{s}$ when $T_c = 793\,\mathrm{K}$.

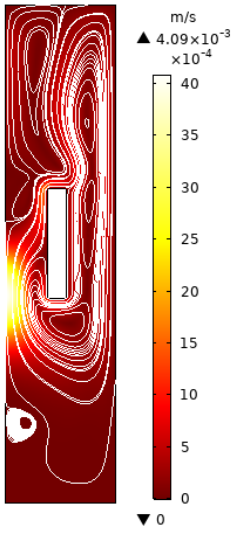

(a) Velocity streamlines.

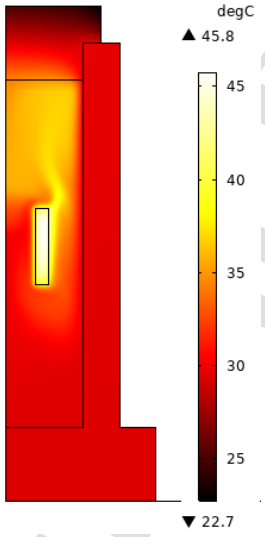

(b) Temperature.

Fig. 5: Distribution of the velocity streamlines (a) and temperature field (b) at $t = 25\,000\,\mathrm{s}$ when $T_c = 393\,\mathrm{K}$.

B. Use of Magnets

In the rest of the paper, T_c is set at $793\,\mathrm{K}$. The objective of this part is to evaluate the impact of a magnet on the cooling efficiency, by changing the distribution of the magnetic field induced by the coil. To achieve this goal, simulated and experimental results obtained in the presence of an actual annular magnet are first compared. This magnet has an axial remanent flux density of $0.2\,\mathrm{T}$. The magnet is localized alongside the aluminum tank. Its section is a rectangle, as shown in Fig. 2 whose characteristics are $r_i = 3.1\ \mathrm{cm}$ (inner radius), $r_e = 7\ \mathrm{cm}$ (outer radius), $H_m = 1.7\ \mathrm{cm}$ (height). After this validation of the numerical model, other configurations are considered to numerically evaluate their respective interest.

1) Comparison of Numerical and Experimental Approaches

For this comparison, the base of the magnet with an axial remanent magnetization is placed at an initial location $Z = 6.5\ \mathrm{cm}$. The time evolution of the temperature is recorded at the two same measurement locations as in the experimental setup. A difference of time constant in the transient regime is observed on Fig. 6, with a shorter thermal diffusion time in the experimental than in the numerical recordings, perhaps related to the homogenized thermal model of the coil. The statistically stationary temperatures are, however, very close for both measurement points. Moreover, both numerical and experimental curves present oscillations for the fluid sensor. Such results that are less present when the magnet is removed (see next point) are related to a fluid flow that is amplified by the presence of the magnet, as it will be shown in the following analysis.

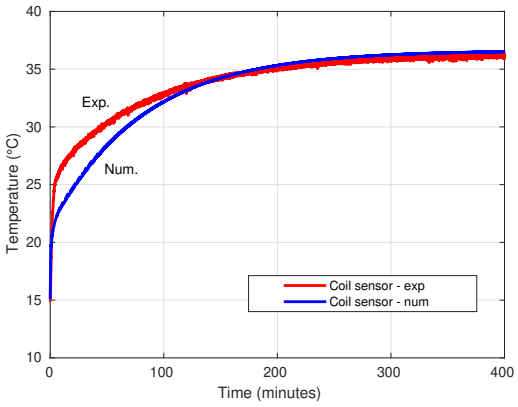

(a) Temperatures at coil sensor.

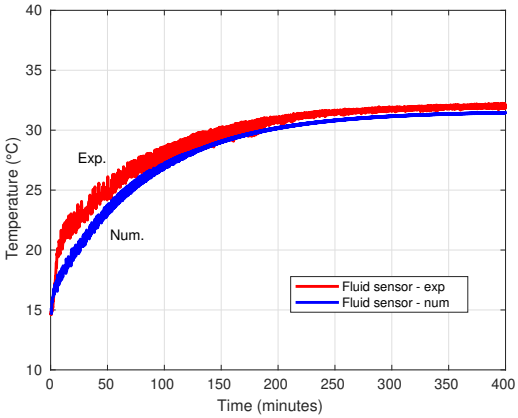

(b) Temperatures at fluid sensor.

Fig. 6: Experimental/numerical cross-validation with the presence of the magnet, $Z = 6.5\ \mathrm{cm}$.

Next, the evaluation of the magnet impact on the cooling process is studied with the comparison between two experi-

mental tests obtained with the same Joule losses; the first one corresponds to the case with the presence of the axial magnet and the other one is the initial configuration without the magnet. The corresponding temperature curves are presented in Fig. 7.

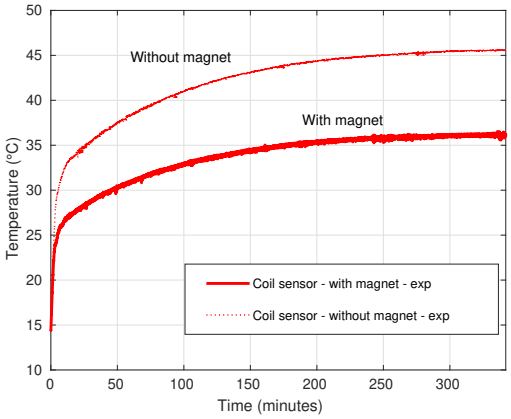

(a) Temperatures at coil sensor.

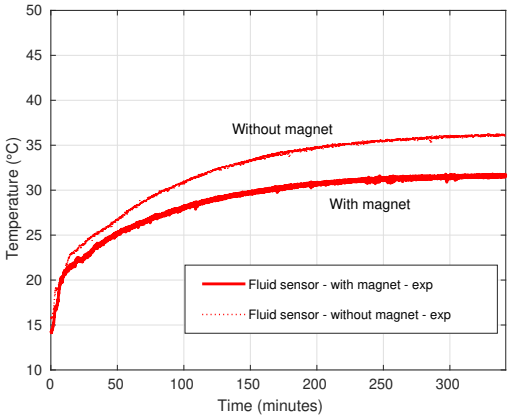

(b) Temperatures at fluid sensor.

Fig. 7: Time evolution of T on the two sensors with and without the axial magnet (experimental), $Z = 6.5$ cm.

It is shown that when the axial magnet is present, the temperature at the top of the solenoid is decreased by about 9 °C. This result is very encouraging because the thermomagnetic convection obtained with the ferrofluid only brings a temperature decrease limited to 2 °C compared to the case with mineral oil. This improvement is due to the modified distribution and amplification of the magnetic distribution in the ferrofluid that increases the magnitude of the magnetic force, and therefore maximizes the flow of the fluid around the coil. The heat exchange with the outside is thus directly boosted.

2) Exploitation of the Numerical Model

The numerical model gives the possibility not only to analyse these results accurately, but also to evaluate the impact of the magnet on the coil maximum temperature, that is not reachable with our test bench. Thus, the magnetic field, velocity and temperature distributions at $t = 25\,000$ s are respectively presented in Fig. 8 and 9.

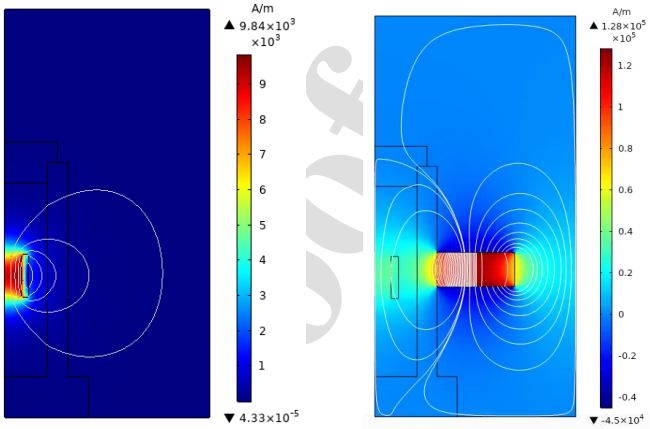

(a) Only coil. (b) Coil and magnet.

Fig. 8: Distribution of the magnetic field intensity (in $\mathrm{A.m^{-1}}$) and flux lines.

According to Fig. 8, the magnetic field generated by the magnet in the ferrofluid clearly dominates the magnetic field due to the coil.

Comparison of the velocity and temperature fields at $t = 25\,000$ s confirms the change in fluid flow around the solenoid, and therefore the effect caused by the external magnet on the cooling. When the magnet is not added, the fluid circulations (see Fig. 4(a)) are due to the presence of the magnetic force acting on the ferrofluid in addition to the thermally induced buoyancy force. Fig. 4(b) shows that the temperature plume emerges from the top of the solenoid, approaches the axis of symmetry (top left edge of the figure), and then bends outward.

When the axial magnet is present, changes in the fluid circulation appear in the part located under the solenoid (see Fig. 9(a)), which amplify the heat removal. The velocity magnitude is increased (its maximum is enhanced by 320%). This is caused by the modification of the field lines and the intensification of the magnetic flux in the fluid. A new thermal plume appears moving downwards and outwards as shown in Fig. 9(b): it is driven by the two lower fluid circulation cells. Another ascending and less active plume is present in the upper part of the tank. It follows the contours of the upper convection cells. In this configuration, the heat exchange surface is increased compared to the case without magnet, where the whole lower half of the device does not contribute to the heat removal. As a consequence of the new fluid flows in the direction of the exchange surface, the maximum temperature of the solenoid is lowered by 5.5 °C. The impact of the magnet is therefore clearly positive in this initial configuration.

3) Optimization of the magnet location

We call optimal positioning of the magnet the search of the vertical location which realizes the higher reduction in the coil maximum temperature. Using the validated numerical model, the optimal position of the same magnet with a vertical remanent flux density field $B_z = -0.2$ T is determined.

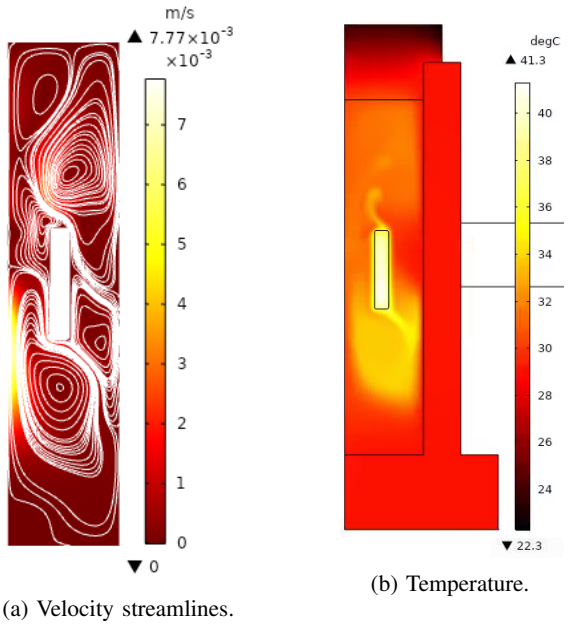

(a) Velocity streamlines. (b) Temperature.

Fig. 9: Distribution of the velocity streamlines (a) and temperature field (b) at $t = 25\,000\,\mathrm{s}$ with coil and annular magnet $B_z = -0.2\,\mathrm{T}$ at $Z = 6.5$ cm.

The maximum temperature evolution in the coil as a function of the vertical position of the magnet is plotted in red in Fig. 10. The temperature values at $t = 25\,000\,\mathrm{s}$ in the fluid at point $(0\ \mathrm{cm}, 8\ \mathrm{cm})$ and at the top of the solenoid $(1\ \mathrm{cm}, 8\ \mathrm{cm})$ are also shown in this figure, respectively with the blue and magenta curves.

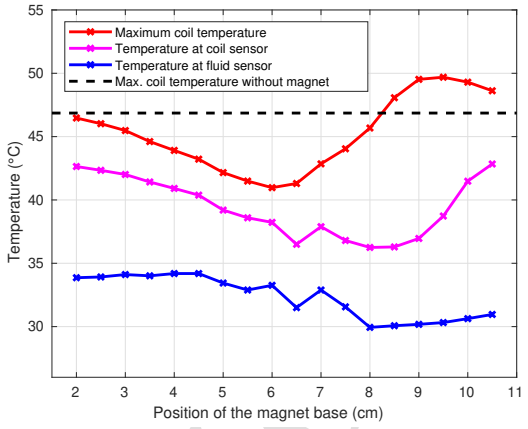

Fig. 10: Temperature on different sensors as a function of the magnet position, with coil and annular magnet $B_z = -0.2\,\mathrm{T}$.

The computation time for each of the required simulations is highly dependent on the magnet position, from about 10 min ($Z = 2$ cm) to more than 63 h ($Z = 6.0$ cm, when the magnet is close to the coil). The laminar fluid flow is shaken up due to periodic vortices that appear in the fluid medium simultaneously with the application of the external magnet. The accelerated fluid circulation undergoes small scales that may be visible at smaller time steps in the computation. By varying the vertical position of the magnet, a $5.9\,^{\circ}\mathrm{C}$ decrease in the maximum temperature of the solenoid is detected for $Z = 6$ cm (base of the magnet).

In this configuration, the distribution of the velocity streamlines is not similar to the one obtained when the magnet is at $Z = 6$ cm, and the maximum velocity magnitude in the fluid domain is enhanced by an order of 36%, see Fig. 11(a). Moreover, the temperature distribution presented in Fig. 11(b) shows again the increased exchange surface with a supplementary fluid circulation at the bottom of the coil. As a consequence, the heat removal presents a small additional improvement compared to the case $Z = 6.5$ cm.

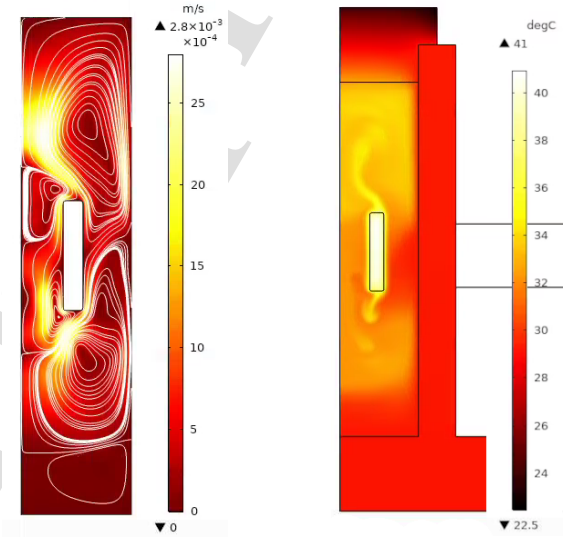

(a) Velocity streamlines. (b) Temperature.

Fig. 11: Distribution of the velocity streamlines (a) and temperature field (b) at $t = 25\,000\,\mathrm{s}$ with coil and annular magnet $B_z = -0.2\,\mathrm{T}$ at $Z = 6$ cm.

The norm of the maximum velocity in the ferrofluid has been calculated as a function of the magnet position (see the blue curve of figure (12)). There is no correlation between V_{max} and the optimal position of the magnet ($Z = 6$ cm). This is related to the fact that the velocity distribution (shown by streamlines) also plays a role: if the velocity norm is maximum where it is not efficient (e.g. towards the bottom left of the coil), then the drop in T is small. On the other hand, the correlation is better with the velocity norm measured just above the coil (at 5 mm) (see red curve in figure (12)).

For a better understanding of the flow dynamical behavior, the time evolution of the RMS velocity has been evaluated for different locations of the magnet (see figure (13)). The root-mean-square (RMS) velocity is given by:

$$V_{RMS} = \left(\frac{1}{\Omega_{bf}} \int_{\Omega_{bf}} u^2 d\Omega_{bf} \right)^{\frac{1}{2}}, \qquad (10)$$

where Ω_{bf} is the base fluid domain.
The figure shows very different time evolutions between the cases of the magnet at the bottom (2 cm, monotonic behavior and low value) and the magnet placed next to the coil (6 cm, highly fluctuated time evolution with a high time-averaged value). Therefore, heat transfer increases with the RMS velocity average value and with its fluctuations.

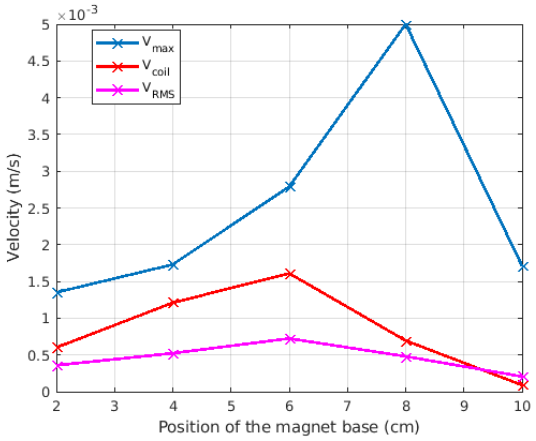

Fig. 12: Velocity on different sensors as a function of the magnet position, with coil and annular magnet $B_z = -0.2\,\mathrm{T}$.

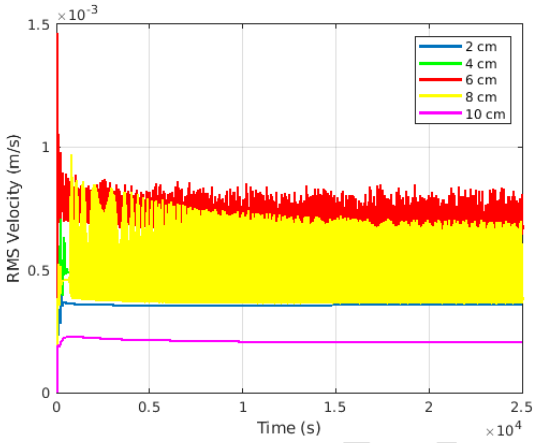

Fig. 13: RMS Velocity at different magnet positions as a function of time, with coil and annular magnet $B_z = -0.2\,\mathrm{T}$.

4) Magnet with other configurations for the remanent magnetization

Other configurations of the remanent magnetization field are evaluated. The vertical remanent flux density field is changed to $B_z = +0.2$ T, see Fig. 14(a) opposite to the one described in the previous section. Then, the effect of a *radial* remanent magnetization with the two possible signs $B_r = \pm 0.2$ T is studied, see Fig. 14(b,c). The magnets shown in this figure are placed at the optimal location found for each magnetization direction, namely at $Z = 6$ cm for $B_z = 0.2$ T (a), at $Z = 3$ cm for $B_r = -0.2$ T (b) and at $Z = 8$ cm for $B_r = 0.2$ T (c).

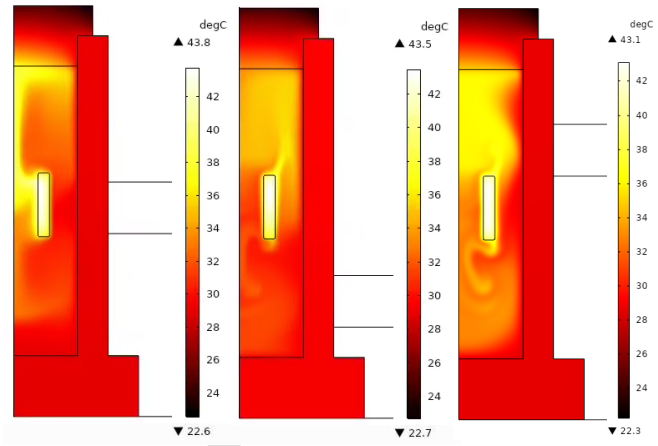

(a) $B_z = 0.2$ T and coil. (b) $B_r = -0.2$ T and coil. (c) $B_r = 0.2$ T and coil.

Fig. 14: Temperature field (in °C) at $t = 25\,000\,\mathrm{s}$ for various configurations of the remanent flux density of the magnet.

The corresponding velocity distributions are presented on Fig. 15 at $t = 25\,000\,\mathrm{s}$ for the three cases of the remanent magnetization.

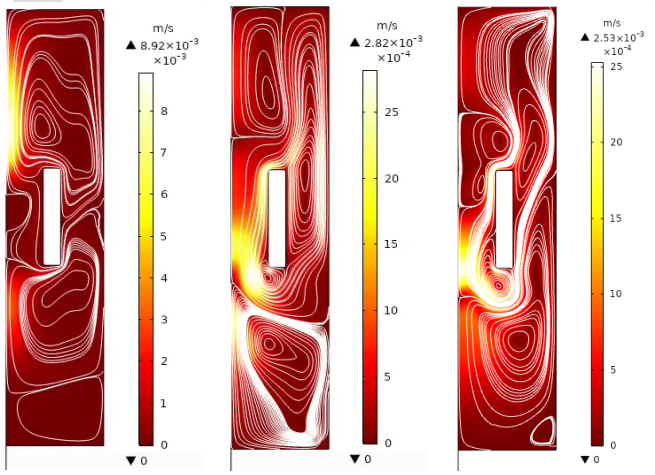

(a) $B_z = 0.2$ T and coil. (b) $B_r = -0.2$ T and coil. (c) $B_r = 0.2$ T and coil.

Fig. 15: Spatial distribution of the velocity magnitude (in $\mathrm{m.s^{-1}}$) and velocity streamlines at $t = 25\,000\,\mathrm{s}$ for various configurations of the remanent magnetization of the magnet.

According to Fig. 14, the decrease in the maximum temperature of the coil, compared to the case without the magnet, goes from about 3 °C ($B_z = 0.2$ T) to 3.8 °C ($B_r = 0.2$ T). In configurations (a) and (b), the temperature decrease seems to be limited by the whole lower half of the device that does not really contribute to the heat removal. This part of the device is almost isothermal, because the additional fluid flow at the bottom of the coil is not present. At first sight, configuration (c) seems to be more interesting, as there is, in this case, a part of the losses removed in the lower direction from the coil. Nevertheless, the heat removal is again limited, this time

because of the temperature distribution in the upper part of the device. Indeed, the hot fluid does not flow in the direction of the cylinder side, but upwards. As a consequence, the exchange surface remains small.

From all these results, the more efficient configuration is the one with a negative axial-magnetized magnet. In the next part, a parametric study is therefore performed with the magnitude of B_z keeping the vertical position of the magnet at the optimal one $Z = 6$ cm.

5) Influence of the magnitude of the vertical remanent flux density of the magnet

The results of a series of simulations are here reported when the magnitude $|B_z|$ of the remanent flux density is varied but the location of the magnet is fixed at $Z = 6$ cm. Fig. 16 presents the maximum temperature obtained in the coil as a function of B_z of the remanent flux density. The maximum temperature in the coil monotonically decreases with the increase of $|B_z|$, and the curve goes towards an asymptote, with a temperature of about 35.3 °C when $B_z = -0.8$T, meaning a 11.5 °C drop. For this study, the larger the remanent flux density, the longer the computation time: about 250 h when $B_z = -0.8$T.

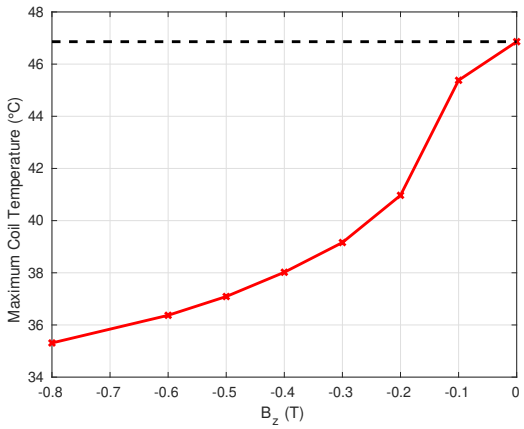

Fig. 16: Maximum temperature in the coil as a function of B_z

Such amplified temperature drop can again be well understood with the analysis of the corresponding temperature distribution, see Fig. 17. With a high remanent flux density, the distribution of the magnetic field in the fluid is mainly due to the magnet. It is observed that with the considered magnet location, the resulting magnetic forces overcome the buoyancy effect when $B_z = -0.8$T and two almost symmetrical heat plumes flow from the upper and lower parts of the coil. As a consequence, the heat flow passes through the entire surface of the tank, maximizing the heat exchange.

IV. Conclusions

The cooling of a ferrofluid-immersed electromagnetic device via thermomagnetic convection has been investigated. The system consists of a winding prototype immersed in a ferrofluid solution based on magnetic nanoparticles. The system has been exposed to an external magnetic field

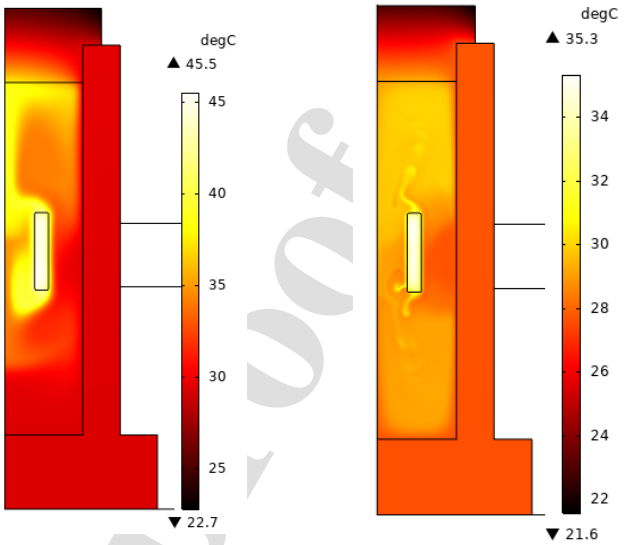

(a) $B_z = -0.1$T. (b) $B_z = -0.8$T.

Fig. 17: Temperature field (in °C) at $t = 25\,000$ s with annular magnet at $Z = 6.5$ cm, $B_z = -0.1$T (a) and $B_z = -0.8$T (b).

generated by an annular magnet placed against the tank.

At first sight, different ferrofluid solutions with various magnetic nanoparticles have been investigated in numerical modeling. The idea is to assess the impact of Curie temperature of magnetic nanoparticles on heat transfer. Simulations have shown that using ferrofluid made of nanoparticles with low Curie temperature may limit the windings' temperature rise and improve the cooling of the electromagnetic device.

An annular magnet, placed against the tank, has been added to the electromagnetic device. The idea is to study the benefit of amplifying the magnetic field distribution in the ferrofluid solution. Experimental measurements have shown that the temperature at the top of the coil is reduced by 9 °C when an axial magnet is added. This has been confirmed numerically using a finite element method in an axisymmetric setting. The numerical results show that using an external magnet intensifies the magnetic force at the top of the coil and then increases the number of vortices in the upper part of the tank. The thermomagnetic convection is thus enhanced.

After this cross-validation between experimental and numerical results, a more exhaustive parametric study was carried out numerically. It is shown that magnetization, orientation, and location of the magnet influence the heat removal process inside the tank.

However, a 3D numerical analysis should be performed in order to confirm the 2D axisymmetric numerical model with the external magnet that has been implemented here.

REFERENCES

[1] Bruce Finlayson. Convective instability of ferromagnetic fluids. *Journal of Fluid Mechanics*, 40:753 – 767, 03 1970.

[2] Harald Engler and S. Odenbach. Parametric modulation of thermomagnetic convection in magnetic fluids. *Journal of physics. Condensed matter : an Institute of Physics journal*, 20:204135, 05 2008.

[3] Elmars Blums, Andrejs Cebers, and M. M. Maiorov. *Magnetic Fluids*. De Gruyter, 2010.

[4] Ranjan Ganguly, Swarnendu Sen, and Ishwar K. Puri. Thermomagnetic convection in a square enclosure using a line dipole. *Physics of Fluids*, 16(7):2228–2236, 2004.

[5] Adrian Lange and Stefan Odenbach. Thermomagnetic convection in magnetic fluids subjected to spatially modulated magnetic fields. *Physics Procedia*, 9:171–175, 2010. 12th International Conference on Magnetic Fluids (ICMF12).

[6] M. Heckert, L. Sprenger, A. Lange, and S. Odenbach. Experimental determination of the critical rayleigh number for thermomagnetic convection with focus on fluid composition. *Journal of Magnetism and Magnetic Materials*, 381:337–343, 2015.

[7] Majid Ashouri and Mohammad Behshad Shafii. Numerical simulation of magnetic convection ferrofluid flow in a permanent magnet–inserted cavity. *Journal of Magnetism and Magnetic Materials*, 442:270–278, 2017.

[8] Iliana Marinova and Valentin Mateev. Thermo-electro-magnetic convection in electrically conductive ferrofluids. In *2019 22nd International Conference on the Computation of Electromagnetic Fields (COMPUMAG)*, pages 1–4, 2019.

[9] Miglenna Todorova, Valentin Mateev, and Iliana Marinova. Ferrofluid brake electromagnetic modeling. In *2021 17th Conference on Electrical Machines, Drives and Power Systems (ELMA)*, pages 1–4, 2021.

[10] Michal Rajňák, Milan Timko, Peter Kopčanský, K. Paulovičová, Jozef Kuchta, Marek Franko, Juraj Kurimsky, Bystrík Dolník, and Roman Cimbala. Transformer oil-based magnetic nanofluid with high dielectric losses tested for cooling of a model transformer. *IEEE Transactions on Dielectrics and Electrical Insulation*, 26(4):1343–1349, 2019.

[11] J. Patel, K. Parekh, and R.V. Upadhyay. Prevention of hot spot temperature in a distribution transformer using magnetic fluid as a coolant. *International Journal of Thermal Sciences*, 103:35–40, 2016.

[12] J. Patel, K. Parekh, and R.V. Upadhyay. Performance of Mn-Zn ferrite magnetic fluid in a prototype distribution transformer under varying loading conditions. *International Journal of Thermal Sciences*, 114:64–71, 2017.

[13] L. Pîslaru-D˘anescu, A. M. Morega, J. B. Dumitru, M. Morega, N. C. Popa, F. D. Stoian, D. Susan-Resiga, S. Holotescu, and M. Popa. Miniature Planar Spiral Transformer With Hybrid, Ferrite, and Magnetic Nanofluid Core. *IEEE Transactions on Magnetics*, 54(10), 2018.

[14] W. Guan, M. Jin, Y. Fan, J.Chen, P. Xin, Y. Li, K. Dai, H. Zhang, T. Huang, and J. Ruan. Finite Element Modeling of Heat Transfer in a Nanofluid Filled Transformer. *IEEE Transactions on Magnetics*, 50(2):2942–2951, 2014.

[15] L. Pîslaru-Dănescu, A. M. Morega, G. Telipan, M. Morega, J. B. Dumitru, and V. Marinescu. Magnetic Nanofluid Applications in Electrical Engineering. *IEEE Transactions on Magnetics*, 49(11):5489–5497, 2013.

[16] Sleimane Nasser El Dine, Xavier Mininger, and Caroline Nore. Heat transfer in a ferrofluid-based transformer: Multiphysics modeling using the finite element method. *IEEE Journal on Multiscale and Multiphysics Computational Techniques*, 7:207–219, 2022.

[17] Peter S.B. Szabo, Miloš Beković, and Wolf-Gerrit Früh. Using infrared thermography to investigate thermomagnetic convection under spatial non-uniform magnetic field. *International Journal of Thermal Sciences*, 116:118 – 128, 2017.

[18] Varun Chaudhary, Zhiping Wang, Ayan Ray, Idapalapati Sridhar, and Raju Ramanujan. Self pumping magnetic cooling. *Journal of Physics D: Applied Physics*, 50:03LT03, 01 2017.

[19] Morteza Hangi and Mehdi Bahiraei. A two-phase simulation for ferrofluid flow between two parallel plates under localized magnetic field by applying lagrangian approach for nanoparticles. *European Journal of Mechanics - B/Fluids*, 74:252–259, 2019.

[20] M. Ghasemian, Z. Najafian Ashrafi, M. Goharkhah, and M. Ashjaee. Heat transfer characteristics of fe3o4 ferrofluid flowing in a mini channel under constant and alternating magnetic fields. *Journal of Magnetism and Magnetic Materials*, 381:158–167, 2015.

[21] M. Yarahmadi, H. Moazami Goudarzi, and M.B. Shafii. Experimental investigation into laminar forced convective heat transfer of ferrofluids under constant and oscillating magnetic field with different magnetic field arrangements and oscillation modes. *Experimental Thermal and Fluid Science*, 68:601 – 611, 2015.

[22] S. Nasser El Dine, X. Mininger, C. Nore, R. Zanella, F. Bouillault, and J. Guermond. Impact of magnets on ferrofluid cooling process: Experimental and numerical approaches. *IEEE Transactions on Magnetics*, 56(1):1–4, 2020.

[23] Ronald E. Rosensweig. *Ferrohydrodynamics*. Dover Publications, 2018.

[24] J. R. MELCHER. *Continuum Electromechanics*. MIT Press, Cambridge, MA, 1981.

[25] Mickaël Petit, Afef Kedous-Lebouc, Yvan Avenas, Wahid Cherief, and Elisabeth Rullière. Etude expérimentale d'un système statique de génération de pression magnétothermique. In *Symposium de Génie Electrique - SGE2014*, Cachan, France, July 2014.

[26] Sleimane Nasser El Dine. *Multi-physics modeling of cooling of power transformers immersed in a ferrofluid*. PhD thesis, Université Paris-Saclay, November 2021.

[27] R. Zanella. *Thermomagnetic convection in ferrofluids : finite element approximation and application to transformer cooling*. PhD thesis, Université Paris Saclay, 2018.

[28] K. Raj and R. Moskowitz. Ferrofluid-cooled electromagnetic device and improved cooling method, 1995. US Patent 5462685.

[29] I. M. Obaidat, B. Issa, B. A. Albiss, and Y. Haik. Temperature Dependence of Saturation Magnetization and Coercivity in $Mn_{0.5}Zn_{0.5}Gd_{0.02}Fe_{1.98}O_4$ Ferrite Nanoparticles. *IOP Conf. Series: Materials Science and Engineering*, 92(012012):1–7, 2015.

Highlights

- **Multiphysic modeling of ferrofluids**

- **New control strategies for improving the thermomagnetic convection**

- **Original transformer cooling system**

Author statement

Sleimane Nasser El Dine:
Conceptualization, Data curation, Formal analysis, Investigation, Software, Visualization, Writing - original draft.

Xavier Mininger:
Funding, Conceptualization, Supervision, Software, Writing - review & editing.

Caroline Nore:
Formal analysis, Methodology, Supervision, Writing - review & editing.

Declaration of interests

☒ The authors declare that they have no known competing financial interests or personal relationships that could have appeared to influence the work reported in this paper.

☐ The authors declare the following financial interests/personal relationships which may be considered as potential competing interests: